

Adaptive Critical Subgraph Mining for Cognitive Impairment Conversion Prediction with T1-MRI-based Brain Network

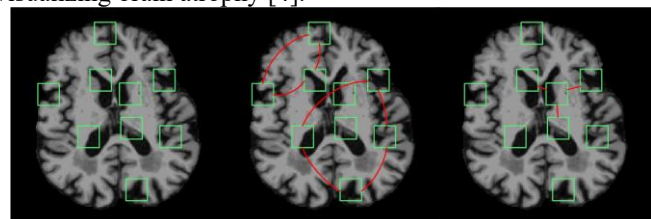
Yilin Leng, Wenju Cui, Bai Chen, Xi Jiang, *Member, IEEE*, Shuangqing Chen, and Jian Zheng, *Member, IEEE*, for the Alzheimer's Disease Neuroimaging Initiative

Abstract—Prediction the conversion to early-stage dementia is critical for mitigating its progression but remains challenging due to subtle cognitive impairments and structural brain changes. Traditional T1-weighted magnetic resonance imaging (T1-MRI) research focus on identifying brain atrophy regions but often fails to address the intricate connectivity between them. This limitation underscores the necessity of focusing on inter-regional connectivity for a comprehensive understand of the brain's complex network. Moreover, there is a pressing demand for methods that adaptively preserve and extract critical information, particularly specialized subgraph mining techniques for brain networks. These are essential for developing high-quality feature representations that reveal critical spatial impacts of structural brain changes and its topology. In this paper, we propose Brain-SubGNN, a novel graph representation network to mine and enhance critical subgraphs based on T1-MRI. This network provides a subgraph-level interpretation, enhancing interpretability and insights for graph analysis. The process begins by extracting node features and a correlation matrix between nodes to construct a task-oriented brain network. Brain-SubGNN then adaptively identifies and enhances critical subgraphs, capturing both loop and neighbor subgraphs. This method reflects the loop topology and local changes, indicative of long-range connections, and maintains local and global brain attributes. Extensive experiments validate the effectiveness and advantages of Brain-SubGNN, demonstrating its potential as a powerful tool for understanding and diagnosing early-stage dementia. Source code is available at <https://github.com/Leng-10/Brain-SubGNN>.

Index Terms—adaptive subgraph mining, loop subgraph, progressive normal cognition, structural brain network, T1-MRI.

I. INTRODUCTION

Progressive cognitive impairment is considered a severe and significant subtype of dementia, including progressive mild cognitive impairment (pMCI) and the less explored progressive normal controls (pNC) [1], [2]. These symptoms represent a continuum of cognitive decline, ranging from subtle changes to more severe impairments. T1-weighted Magnetic resonance imaging (T1-MRI) has emerged as a crucial non-invasive, radiation-free modality for early dementia assessment [3]. It offers superior soft tissue contrast, ideal for identifying and visualizing brain atrophy [4].



(a) critical regions (b) loop connectivity (c) neighbor connectivity

Fig. 1. There are some changes in brain through cognitive impairment. (a) critical regions related to atrophy or some other lesion, (b) closed-loop mechanisms in brain self-regulation, (c) local neighbor connectivity.

Recent deep learning (DL) methods utilizing T1-MRI [5]-[7] have advanced the assessment of brain atrophy, holding potential for intelligent assessment of cognitive impairment. However, despite the state-of-the-art (SOTA) performance of Convolutional Neural Networks (CNNs), current T1-MRI-based methods often compromise the global brain shape and topology [8]-[11]. This is due to methods that reduce irrelevant context by cropping equal-sized patches [8] or focusing solely on discriminative anatomical brain regions, such as hippocampus [12], [13]. To address these challenges, several studies [13]-

This work was supported in part by the National Natural Science Foundation of China (Nos.62371499, U23A20483), and in part by the Department of Science and Technology of Shandong Province under Grants (Nos.ZR202211070272, SYS202208). Corresponding author: Shuangqing Chen (email: sznaonao@163.com) and Jian Zheng (email: zhengj@sibet.ac.cn).

Y. Leng, W. Cui, C. Bai and J. Zheng are with the Department of Medical Imaging, Suzhou Institute of Biomedical Engineering and Technology, Chinese Academy of Sciences, Suzhou, 215163, China.

W. Cui, C. Bai and J. Zheng are also with School of Biomedical Engineering (Suzhou), Division of Life Sciences and Medicine, University of Science and Technology of China, Hefei, 230026, China.

S. Chen is with the Department of Radiology, the Affiliated Suzhou Hospital of Nanjing Medical University, Suzhou, 211103, China.

X. Jiang is with the Clinical Hospital of Chengdu Brain Science Institute, MOE Key Lab for Neuroinformation, School of Life Science and Technology, University of Electronic Science and Technology of China, Chengdu, 611731, China.

Data used in preparation of this article was obtained from the Alzheimers Disease Neuroimaging Initiative (ADNI) database (<http://www.adni-info.org/>). The investigators within the ADNI contributed to the design and implementation of ADNI and/or provided data, but did not participate in analysis or writing of this report. A complete listing of ADNI investigators can be found at http://adni.loni.usc.edu/wp-content/uploads/how_to_apply/ADNI.

[16] have constructed brain networks incorporating shaped-related priors. However, these methods detect fuzzy patterns and struggle to capture precise distinguishable information effectively. Therefore, localizing critical structures (e.g., subgraphs) is essential for analyzing and interpreting changes in the brain.

Preserving and extracting maximum information is essential for high-quality feature representations, particularly in pinpointing the spatial distribution of effects caused by local structural changes. The advancement of Graph Neural Networks (GNNs) has broadened applications across various fields, including human networks [17], traffic analysis [18], and drug discovery [19]. While numerous studies [20]-[24] have employed GNNs for analyzing human brain networks, most [25]-[30] focus on graph or node classification tasks, overlooking critical subgraphs. Existing subgraph mining methods, like graph kernels [31], [32], decompose pre-defined structures from the original graph, demonstrating competitive performance in specific domains. However, their handcrafted and heuristic nature limits their flexibility and generalization capabilities. Meanwhile, recent graph transformers [23], [34] struggle to identify structural similarities between nodes, limiting their ability to identify critical edges. Therefore, it remains a challenge to adaptively identify critical structures both locally and globally without fixed rules or prior knowledge.

Recent studies [35], [36] highlight the roles of specific brain regions in neurofeedback control and reward processing, emphasizing the importance of underlying closed-loop mechanisms in brain self-regulation. These insights inform the critical need for loop information mining in neurological research. Moreover, the inherent rich club [37] and small-world [38] properties of brain networks, underlining local and long-range connectivity, are underexplored in T1-MRI-based research. These properties are crucial for understanding the complex interplay of brain regions in cognitive disorders. Consequently, there is a significant gap in the development of subgraph mining methods that can adaptively explore data-specific and task-specific critical structures in brain networks, i.e., subgraphs of arbitrary size and shape.

In this paper, we present a novel approach called Brain-SubGNN for early diagnosis of cognitive impairment, addressing these challenges with a brain subgraph neural network. The pipeline of our framework is illustrated in Fig. 1, aims to enhance the identification of critical structures and improve interpretability. Firstly, we adopt a unified graph representation that adaptively allocates nodes to discriminative regions, thereby accounting for varying atrophic patterns and connectomes across individuals. Secondly, we design a subgraph mining network named Brain-SubGNN to acquire graph topology information and mine critical subgraphs without prior knowledge. We innovatively incorporate reinforcement learning (RL) based subgraph mining modules for dynamic identification of critical neighbor and loop subgraphs associated with cognitive impairment. Additionally, we compute mutual information (MI) between all mined subgraphs and the global graph to reinforce

subgraphs representation.

The experimental results demonstrate that our novel approach outperforms several SOTA methods in predicting the conversion of MCI (i.e., sMCI vs. pMCI). Notably, we make a pioneering contribution by successfully predicting the likelihood of future conversion from Normal Controls to MCI (sNC vs. pNC), presenting promising results. Our contributions are illustrated as followings:

- This work constructs a complete multi-resolution framework that includes adaptive brain network construction, critical region and structure mining.
- Brain-SubGNN is a data and task-driven subgraph mining network. A loop and a neighbor subgraph mining module are designed based on the properties of brain networks to detect changes in self-regulation and local effects associated with cognitive degradation.
- This study reports a remarkable achievement in identifying individuals who will develop cognitive impairment within three years from normal individuals (pNC vs. sNC) on publicly available datasets. This result suggests the potential to further advance early diagnosis and intervention of cognitive impairment.

II. RELATED WORKS

A. Methods on T1-MRI and Brain Networks

Recently, DL methods have demonstrated remarkable performance in computer vision tasks, prompting their exploration in computer-aided diagnosis of neurodegenerative diseases. Four primary types of DL methods are illustrated as: 1) *Whole-image-based methods*: a widely employed class of DL techniques, extract spatial contextual information directly from original images [7]; 2) *ROI-based methods*: partition brain imaging data into regions of interest (ROI) using templates like automatically Automated Anatomical Labeling (AAL) [39] or manual anatomy for analysis and classification [40]; 3) *Slice-based methods*: divide the image into slices and employ a 2D network for classification [10]; 4) *Patch-based methods*: crop patches or use attention mechanisms to focus on regions affected by early dementia in the MR images [5], [6], [9].

The brain's complexity and diversity make graphical representation ideal for analyzing MR images' intricate backgrounds and heterogeneous lesions. While CNNs are proficient with Euclidean data, they struggle with non-Euclidean data like the brain's macrostructural complexity [41]. Graph-based methods transform brain MR images into graphs for region identification and connection analysis overcome the challenge associated with applying fundamental mathematical procedures. In the realm of fMRI-based research [21]-[25], [30], such methods have been widely employed to construct brain function connection network for the disease processing analysis, achieving SOTA performance cross multiple datasets. However, applying GNNs to T1-MRI is still in development due to the absence of direct correlation between regions.

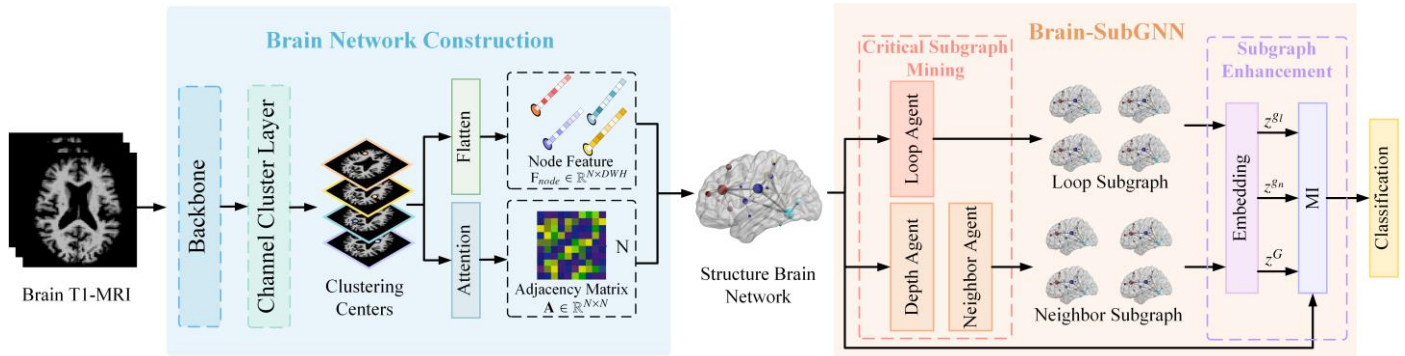


Fig. 2. The workflow of our proposed method. It assesses brain disorders in three steps: 1) constructing adaptively data-specific and task-specific structural brain networks with both dynamic nodes and dynamic connections; 2) mining critical subgraphs through two Modules, which adaptively mine local loop and neighbor subgraphs of task-oriented, individually heterogeneous and arbitrarily size and shape; 3) encoding loop and neighbor subgraphs, and fuses subgraphs information with global graphs using shallow graph convolution for downstream tasks.

B. Brain Subgraph Mining

The success of GNNs in analyzing graph-structured data [17]-[19] has led to deep models predicting brain diseases by learning graph structures of brain networks [27]-[30]. Conventional approaches, like graph kernels (e.g., temporal random walk [42], [43], shortest path [44], neighborhood representation [45] and subgraph sketching), decompose pre-defined structures from the original graph, demonstrating competitive performance in specific domains. However, their handcrafted and heuristic nature limits their flexibility and generalization capabilities. Meanwhile, recent graph transformers [46] struggle to identify structural similarities between nodes, limiting their ability to identify critical edges. Therefore, detecting data-specific and task-specific critical structures at both local and global scales in brain network without fixed rules or prior knowledge remains a problem.

Recently, RL has been incorporated into various graph mining tasks [47], such as graph representation learning [48], graph adversarial attack [49], relational reasoning [50], GNN explainer [51], and combination optimization [52]. RL is a fundamental branch of machine learning where agents learn to make optimal decision sequentially within an environment. The Mathematical framework of Markov decision process (MDP) is commonly employed to formulate RL as a sequential decision process [53]. Similar to Brain-SubGNN, some methods [54], [55] use RL to identify critical structures and enhance graph learning. For instance, Lai et al. [48] employed the Deep Q-Network (DQN) [56] to determine the optimal number of aggregation iterations for different nodes, while Gao et al. [57] used RL to search for optimal GNN architectures, showing RL's growing application in GNN optimization and development.

In conclusion, existing GNNs with RL focus on identifying critical relations or improving GNN architectures for node-level tasks. However, limited research has been conducted to advanced RL for identifying more complex critical structures in graph-level tasks.

III. METHODS

A. Dynamic Brain Network Construction

To construct brain networks from T1-MRI data, we utilize methods from our prior work [26] to identify discriminative regions and examine their connectivities. Each subject is conceptualized as a graph $G = \{V, A\}$, where V represents vertices corresponding to discriminative regions, and A denotes the edges reflecting the relationships between these regions. This results in a brain network adaptively tailored to the specific characteristics of each subject.

1) *Selection of Nodes*: We first obtain abundant feature maps using a powerful encoder, then cluster the feature maps of multiple channels to obtain discriminative feature maps as nodes. Specifically, peak responses coordinates of feature maps are defined as the candidate prototypes inspired by [58], then feature maps with representative positions are selected as discriminative ones by K-means [59]. The position vectors of feature maps over all training images are expressed as:

$$[t_x^1, t_y^1, t_z^1, \dots, t_x^\Omega, t_y^\Omega, t_z^\Omega] \quad (1)$$

where $[t_x^i, t_y^i, t_z^i]$ denotes the peak response coordinate of the feature map corresponding to the i -th images, and Ω is the number of training images. Clustering these peak responses using K-means yields N clustering centers, serving as nodes $V = \{v_1, v_2, \dots, v_N\}$ for graph construction, where v_j is the feature map of the j -th channel clustering center.

To integrate clustering process into the network training and optimize the results, we employ a channel clustering layer (CCL) with prototype contrastive learning into network training. Specifically, the CCL comprises two fully connected layers (FCs) and a skip connection, encouraging each channel cluster to be compact internally and have significant inter-class differences from other clusters. Optimization is performed using the prototype contrastive learning [60] loss function:

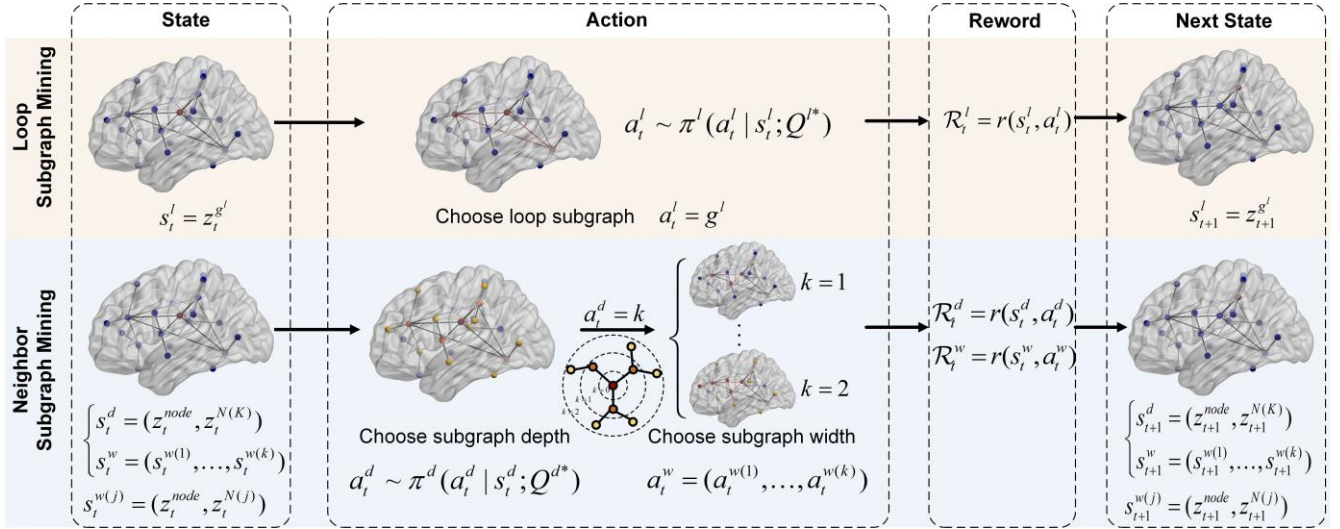


Fig. 3. The workflow of subgraph mining module. For a given center node, 1) the LSRM generates an action a_t^l by policy π^l to detect the critical loop subgraph; 2) the NSRM generates an action a_t^d by policy π^d to choose the depth of subgraph, then the policy π^w generates an action a_t^w to choose the width of subgraph.

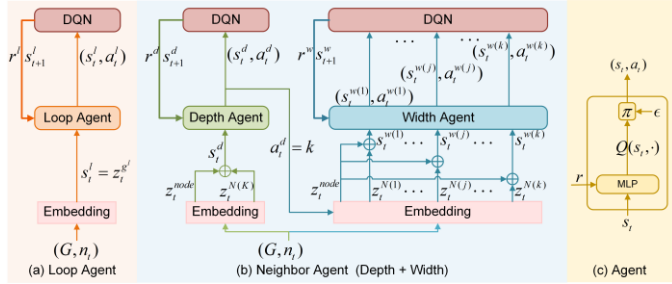


Fig. 4. The agents of subgraph mining module.

$$\mathcal{L}_{ccl} = -\frac{1}{N_c} \sum_{i=1}^{N_c} \sum_{u \in K_i} \log \frac{\exp(u \cdot \gamma_i / \phi_i)}{\sum_{j \neq i} \exp(u \cdot \gamma_j / \phi_j)} \quad (2)$$

$$\phi_i = \frac{\sum_{u \in K_i} \|u - \gamma_i\|_2}{|K_i| \cdot \log(|K_i| + \alpha)} \quad (3)$$

Where N_c is the number of clusters, K_i , γ_i , and ϕ_i denote the set of all elements, the cluster center (prototype), and the concentration estimation of the i -th cluster, respectively. α is a smoothing parameter to prevent small clusters from having overly-large ϕ . The cluster concentration ϕ measures the closeness of elements in a cluster. \mathcal{L}_{ccl} compels all elements u in K_i to be close to their cluster center γ_i and away from other cluster centers.

In this way, a data- and task-oriented discriminative regions are automatically identified as nodes for each subject.

2) **Generation of Edges:** To establish adaptive inter-regional correlations, we employ an attention mechanism [61] for edge connection in each image, allowing nodes to exchange features along related graph edges. Specifically, the clustering feature $F_{ccl} \in \mathbf{R}^{N \times D \times W \times H}$ obtained from CCL are processed through three separate FCs to compute attention scores between each pair of prototypes. The edge connection is stored by the

adjacency matrix $A \in \mathbf{R}^{N \times N}$ to obtain the output of self-attention layer:

$$A = \text{Attention}(Q, K, V) = \text{softmax}\left(\frac{QK^T}{\sqrt{d_k}}\right)V \quad (4)$$

where $Q \in \mathbf{R}^{N \times d_k}$, $K \in \mathbf{R}^{N \times d_k}$ and $V \in \mathbf{R}^{N \times N}$ denote query, key, and value, respectively. d_k represents the dimension of Q and K . N is the number of discriminative regions.

Ultimately, by employing the prototypes as nodes and correlations as edges, we construct a disease-related individualized structural brain network with both adaptive nodes and adaptive connections.

B. Critical Brain Subgraph Mining

To adaptively mine subgraphs of arbitrary size and shape without supervision, we develop two modules: the Loop Subgraph Reinforced Mining module (LSRM) and the Neighbor Subgraph Reinforced Mining module (NSRM). Both are designed to model the subgraph mining approach as a Finite Horizon Markov Decision Process (MDP), enabling autonomous discovery of critical subgraphs guided by downstream task feedback. As depicted in Fig.3, our method begins by selecting a set of seed nodes as the central nodes of the subgraph. LSRM with its loop agent, mines loop subgraphs that contain n_i , facilitating the analysis of discriminative connectivity information. Concurrently, NSRM with its depth and width agents, mines the neighbor subgraphs, focusing on local neighborhoods to gather information. These two approaches allow for a comprehensive analysis of both loop structures and neighboring interactions, enhancing our understanding of brain connectivity patterns.

1) **Loop Subgraph Reinforced Mining Module:** We first sample a set of seed nodes $V_{seed} = \{n_i\}_{i=1}^M$ as central nodes of the subgraph, and then pick the graph around these seed nodes.

For each central node n_i , an encoder initially transforms node features into node codes.

The loop subgraphs containing n_i are then mined with a loop agent. The loop agent operates by generating a series of actions $\{a_i^{l(j)} \mid j \in [0, \delta] \text{ and } j \in \mathbb{Z}\}$ to select loop subgraphs g^l according to the policy $\pi^l(s_i^l)$, where δ denotes the total number of subgraphs. Specifically, the loop agent is defined by four components $(\mathcal{S}^l, \mathcal{A}^l, \mathcal{R}^l, \mathcal{T}^l)$: **1) State** \mathcal{S}^l consists of the embedding of all nodes of the currently selected subgraph, denoted as $s_i^l = \{z_i^{g^l}\}$, where g^l is the currently selected subgraph; **2) Action** \mathcal{A}^l consists of a series of subgraphs selecting the action $\{a_i^{l(j)} \mid j \in [0, \delta] \text{ and } j \in \mathbb{Z}\}$ for selecting the current subgraph g_i^l and δ representing the number of all subgraphs; **3) Reward** \mathcal{R}^l is defined as a discrete reward function $r(s_i^l, a_i^l)$, since it is unavailable to determine the state and its accumulated reward in GNN after each action is taken. As illustrated in (5), reward determines whether the reward of (s_i^l, a_i^l) is positive based on whether the predicted label \hat{y}_i is equal to the true label y ; **4) Transition** \mathcal{T}^l samples the next subgraph after the current subgraph is determined, until δ subgraphs are sampled.

$$r(s_i^*, a_i^*) = \begin{cases} +0.5, & \text{if } \hat{y}_i = y \\ -0.5, & \text{if } \hat{y}_i \neq y \end{cases} \quad (5)$$

After completing the setup of loop agent, to achieve the overall steps of maximizing the expected total reward by starting from the current state, we apply the model-free algorithm DQN to learn the optimal policy for the agents, which is completely alternative. Specifically, DQN learns the state-action values $Q^l(s^l, a^l)$ by using a deep neural network, we therefore train Q^l functions for loop agent based on (6):

$$Q^l(s^l, a^l) = \mathbb{E}_{s_i^l} \left[\mathcal{R}(s^l) + \gamma^l \max_{a_i^l} (Q^l(s^l, a^l)) \right] \quad (6)$$

where $\gamma^l \in [0, 1]$ is the discount factors of future reward. Then the policies π^l are obtained by a ϵ -greedy policy with an explore probability ϵ as:

$$\pi^l(a_i^l \mid s_i^l; Q^{l*}) = \begin{cases} \text{random action,} & p = \epsilon \\ \arg \max_{a_i^l} Q^{l*}(s_i^l, a_i^l), & p = 1 - \epsilon \end{cases} \quad (7)$$

$$\pi^l(G) \Rightarrow g_j^l \quad (8)$$

where π^l is used to explore new states by choosing random actions with probability ϵ , p is the probability of current action. Briefly, we first mine all the loop subgraphs from the original graph G and input them to π^l one by one as (8) to further analyze discriminative brain connectivity information. Notably, the brain loops here are not clinically disorder in function but are closed connections connected by disorder task-related brain regions. Besides, some graphs may not contain loop subgraphs.

2) Neighbor Subgraph Reinforced Mining Module: To mine subgraphs of arbitrary size and shape, we split the NSRM module into depth and width agents to mine the appropriate depth and width for subgraph. Specifically, for node n_i in state

\mathcal{S}^l , the depth agent generates an action a_i^d according to the policy $\pi_i^d(*)$ to define the depth h_i for the subgraph of node n_i . When $h_i = a_i^d$, the width agent will generate a series of actions $\{a_i^{w(i)} \mid i \in [1, h] \text{ and } i \in \mathbb{Z}\}$ for sampling the member nodes of subgraph within k-hop neighbors of n_i hop by hop. Our two agents are described in detail below.

The depth agent is denoted a tuple $(\mathcal{S}^d, \mathcal{A}^d, \mathcal{R}^d, \mathcal{T}^d)$: **1) State** \mathcal{S}^d is denoted as $s_i^d = (z_i^{node}, z_i^{N(K)})$, comprising the embedding z_i^{node} of current central node n_i and the context embedding $z_i^{N(K)}$ of its k-hop neighbors. $z_i^{N(K)}$ is the average vector of all nodes in the k-hop neighborhood of current node n_i , and K is the hyperparameter that limits the maximum subgraph depth; **2) Action** \mathcal{A}^d consists of a series of depth selection actions $\{a_i^d\}$ for selecting the maximum depth of the subgraph from node n_i , where $a_i^{d(i)} \in [1, K]$ is a positive integer; **3) Reward** \mathcal{R}^d is defined as a discrete reward function $r(s_i^d, a_i^d)$ illustrated in (8) the reward of (s_i^d, a_i^d) is positive when the predicted label \hat{y}_i is equal to the true label y ; **4) Transition** \mathcal{T}^d samples the next center node from the seed nodes as the next state s_{i+1}^d once the depth of the current subgraph is determined, until N subgraphs are sampled.

The width agent is denoted as $(\mathcal{S}^w, \mathcal{A}^w, \mathcal{R}^w, \mathcal{T}^w)$ in a similar way: **1) State** \mathcal{S}^w is denoted as a sires of $\{s_i^{w(k)}\}$, which consists of the spatial embedding $z_i^{g^{k-1}}$ of the subgraph of the current center node n_i and the context embedding $z_i^{N(K)}$ in the n_i 's k -th hop. The $z_i^{g^{k-1}}$ is the average vector of all nodes in the current $(k-1)$ -hop subgraph, and $z_i^{g^1}$ is initialized to the embedding representation of the central node n_i , $z_i^{N(K)}$ is the average vector of all nodes in the k -th hop neighbors of node n_i ; **2) Action** \mathcal{A}^w consists of a series of width selection actions $a_i^w = \{a_i^{w(i)} \mid i \in [1, k] \text{ and } i \in \mathbb{Z}\}$ when $k = a_i^d$, where $a_i^{w(i)}$ represents the action in i -th hop for width sampling; **3) Reward** \mathcal{R}^w is same as \mathcal{R}^d , illustrated in (5); **4) Transition** \mathcal{T}^d represents the current subgraph and the next hop node as the next state s_{i+1}^w after the current subgraph depth is determined, until all k-hop nodes of the subgraph are completed sampling.

After completing the setup of both agents, we apply the DQN to learn the state-action values Q^d and Q^w (Here denoted uniformly as Q) by using a deep neural network for depth and width agents:

$$Q(s, a) = \mathbb{E}_s \left[\mathcal{R}(s') + \gamma \max_{a'} (Q(s', a')) \right] \quad (9)$$

where $\gamma^d \in [0, 1]$ and $\gamma^w \in [0, 1]$ is the discount factors of future reward. Then the policies π^d and π^w are obtained by a ϵ -greedy policy with an explore probability ϵ as:

$$\pi(a_i | s_i; \mathcal{Q}^*) = \begin{cases} \text{random action,} & p = \epsilon \\ \arg \max_a \mathcal{Q}^*(s_i, a_i), & p = 1 - \epsilon \end{cases} \quad (10)$$

where π^d and π^w are used to explore new states by choosing random actions with probability ϵ . Briefly, as (11), we first input the original graph G and nodes n_i to π^d to get the subgraph depth optimum d_i , and then input G , n_i and d_i to π^w to get the final selected nodes of the subgraph, thus obtaining the neighborhood subgraph representing the neighborhood context information.

$$\pi^d(G, n_i) \Rightarrow d_i, \quad \pi^w(G, n_i, d_i) \Rightarrow g_i \quad (11)$$

C. Critical Brain Subgraph Mining

While subgraphs provide critical representation of the global graph, they may not fully capture important global properties (i.e., topological features, inter-subgraph connections) when used directly for downstream classification tasks. To address this limitation, we have implemented a subgraph enhancement module. This module incorporates a mutual information (MI) maximization mechanism to enhance subgraph representation. We choose the Jensen-Shannon divergence (JSD) [62]-[63] estimator, for its efficiency in distinguishing samples from joint and marginal distributions and its insensitivity to negative sampling strategies. This makes it particularly suitable for our multi-agent RL framework.

Specifically, this module aims to maximize MI between subgraph representations (loop and neighbor subgraph) and their corresponding global graph representations. The MI for loop subgraph I_l and neighbor subgraph I_n (Here denoted uniformly as I) can be expressed as:

$$I(z^s; z^G) = \mathbb{E}_{\mathbb{P}}[-sp(-\mathcal{T}(z^s; z^G))] - \mathbb{E}_{\mathbb{P}}[sp(\mathcal{T}(z^s; z^G))] \quad (12)$$

$$sp(x) = \log(1 + e^x) \quad (13)$$

where z^s represent the embedding of subgraph, z^G and $z^{G'}$ are the global graph embeddings of the corresponding instance and another instance in the current batch. G' is sampled from $\mathbb{P} = \mathbb{P}$, and $sp(x)$ is the soft-plus function. The total MI I_{sum} is the weighted sum of the two subgraphs' MIs:

$$I_{sum} = I_n + u(\delta)I_l \quad (14)$$

where δ is the number of loop subgraphs, $u(*)$ is the step function. The loss for subgraph enhancement module combines the losses from both loop and neighbor subgraph representations:

$$\mathcal{L}_{MI} = \mathcal{L}_{MI}^n + \mathcal{L}_{MI}^l = \frac{1}{N + N_{neg}} \left(\sum_{g \in G} \log(\mathcal{D}(z^s; z^G)) + \sum_{g \in G} \log(1 - \mathcal{D}(z^s; z^{G'})) \right) \quad (15)$$

where \mathcal{L}_{MI}^n and \mathcal{L}_{MI}^l are the loss of neighbor and loop subgraph representation, $\mathcal{D}(*)$ is a discriminator leveraging a neural network. N and N_{neg} are the number of chosen subgraph and negative samples. In this context, negative samples are defined as global graphs other than the subgraph's corresponding global

TABLE I
DEMOGRAPHIC INFORMATION OF THE SUBJECTS. THE GENDER IS PRESENTED AS MALE/FEMALE, AGE AND EDUCATION YEARS ARE PRESENTED AS MEAN \pm STANDARD DEVIATION

Dataset	Type	Num	Gender(M/F)	Age(year)	Education
ADNI-1	sMCI	197	126/71	75.03 \pm 7.36	15.59 \pm 3.10
ADNI-1	pMCI	108	68/40	77.59 \pm 7.57	15.73 \pm 2.61
ADNI-2	sMCI	251	138/113	71.46 \pm 7.31	16.32 \pm 2.70
ADNI-2	pMCI	99	55/44	76.72 \pm 6.39	16.05 \pm 2.66
NACC	sNC	281	74/207	66.94 \pm 8.60	16.00 \pm 2.39
NACC	pNC	187	64/123	75.44 \pm 10.34	16.34 \pm 9.15

graph, aligning with contrast learning principles to encourage subgraph embeddings to align closely with their corresponding global graph embeddings while distancing from other global graph embeddings.

D. Optimization Process

To achieve optimized results, we unify the training of brain network construction and subgraph mining. Specifically, optimization process contains: 1) pretraining the backbone to initialize feature extraction; 2) clustering feature channels with K-means; 3) pretraining CCL to align with the k-means operation; 4) freezing the subgraph mining enhancement module of graph convolution, training the combined backbone, CCL and Brain-SubGNN to encode and optimize the brain network graph; 5) jointly training all modules of Brain-SubGNN for subgraph mining and enhancement. The overall loss function is defined as:

$$\mathcal{L} = \mathcal{L}_{ccl} + \mathcal{L}_g + \beta \mathcal{L}_{MI} \quad (16)$$

where \mathcal{L}_{ccl} is the channel clustering loss described in (2), \mathcal{L}_g is the cross-entropy loss for global graph classification, \mathcal{L}_{MI} is the MI loss between the subgraph and the global graph, and β is the hyper-parameter controlling the impact of \mathcal{L}_{MI} .

IV. EXPERIMENTS AND RESULTS

A. Materials and Preprocessing

The data utilized in this study are from three publicly available database: Alzheimer's Disease Neuroimaging Initiative 1 and 2 (ADNI-1, ADNI-2) [64], National Alzheimer's Coordinating Center (NACC) [65], including 1.5T, 2T and 3T T1-weighted MRI data. We collect 1123 subjects in all datasets, including 448 sMCI, 207 pMCI, 281 sNC, and 187 pNC. Note that for subjects appearing in multiple datasets of ADNI (e.g., ADNI-1 and ADNI-2), we only keep the former. Demographic details of the subjects are shown in Tab.I. The T1-MRI data underwent preprocessing following our previous work [26].

B. Implementation Details

We choose convmixer [66] as the backbone with convolutional kernel=5, depths=5 and channels=2048. K-means is set with cluster centers $N_c=16$, and the CCL is a two-layer FCs implementing prototype contrast learning smooth with parameter $\alpha=10$ following [67]. The Brain-SubGNN consists of a two-layer DenseGCN [68], a two-layer Graph Isomorphism Network (GIN) [69] two subgraph mining module to implement original graph encoding, subgraph encoding, critical subgraph mining and subgraph enhancement, respectively.

TABLE II
COMPARISON OF OUR METHOD WITH CURRENT SOTA METHODS FOR MCI
CONVERSION PREDICTION ON ADNI-2, OBTAINED BY THE MODELS TRAINED ON
ADNI-1

Method	ADNI1	ADNI2	ACC	SEN	SPE	AUC
LDMIL [5]	226/167	239/38	0.769	0.421	0.824	0.776
H-FCN [8]	226/167	239/38	0.809	0.526	0.854	0.781
HybNet [6]	226/167	239/38	0.827	0.579	0.866	0.793
AD ² A [9]	147/165	253/88	0.780	0.534	0.866	0.788
DSNet [7]	147/165	256/89	0.762	0.770	0.742	0.818
MSA3D [10]	229/167	241/75	0.801	0.520	0.856	0.789
M ² FAN [11]	165/175	323/109	0.815	0.670	0.864	0.817
DH-ProGCN [26]	197/108	251/99	0.849	0.647	0.928	0.845
Ours	197/108	251/99	0.869	0.727	0.924	0.882

The maximum depth of neighbor subgraph=3, the number of mined subgraphs is chosen according to the size of the graph. The β of MI loss is set as 0.8. The Q function of DQN is set to a 5-level MLP with (128, 256, 512, 256, 128) hidden units, and the ϵ of the ϵ -greedy policy decreases from 1.0 to 0.2 at a rate of 0.95 per 100 steps according to a linear scheduler.

The model is trained for 300 epochs with initial learning rates of $1e^{-4}$, $1e^{-6}$ and $1e^{-2}$ for the backbone, CCL and Brain-SubGNN, respectively. The learning rates are decreased by a factor of 10 every 100 epochs. Evaluation metrics include accuracy (ACC), sensitivity (SEN), specificity (SPE), and area under the curve (AUC). We use Python and PyTorch package, and run the network on a single NVIDIA GeForce 3090 GPU.

Our model is evaluated on two tasks, NC conversion prediction (sNC vs. pNC) and MCI conversion prediction (sMCI vs. pMCI). As the NC data is derived from a single dataset and the MCI data comes from two distinct datasets, we therefore perform a five-fold cross-validation on sNC vs. pNC and sMCI vs. pMCI tasks in all experiments, and an independent validation on sMCI vs. pMCI task for SOTA comparison.

C. Comparison with the State-of-the-Art Methods

After in-depth survey, we find there are no Deep Learning study on sNC vs. pNC classification using T1-MRI images. Therefore, we here focus on presenting SOTA comparison for sMCI vs. pMCI classification. Eight SOTA methods are used for comparison: 1) LDMIL [5] captured both local information conveyed by patches and global information; 2) H-FCN [8] implemented three levels of networks to obtain multi-scale feature representations which are fused for the construction of hierarchical classifiers; 3) HybNet [6] assigned the subject-level label to patches for local feature learning by iterative network pruning; 4) AD²A [9] located discriminative disease-related regions by an attention modules; 5) DSNet [7] provided disease-image specificity to an image synthesis network; 6)

TABLE III
EFFECTS OF DIFFERENT TYPES OF NODES AND EDGES

	dynamic		5-fold validate on ADNI-1&2			
	node	edge	ACC	SEN	SPE	AUC
sMCI vs. pMCI	ROI-based		0.774	0.606	0.841	0.793
			0.798	0.695	0.804	0.803
	✓		0.800	0.668	0.854	0.831
	✓	✓	0.810	0.696	0.857	0.831
sNC vs. pNC	ROI-based		0.847	0.828	0.854	0.916
			0.851	0.816	0.875	0.921
	✓		0.870	0.840	0.890	0.927
	✓	✓	0.880	0.861	0.893	0.922

TABLE IV
EFFECTS OF DIFFERENT SUBGRAPH MINING AND ENHANCEMENT STRATEGIES

	strategies			5-fold validate on ADNI-1&2			
	Neighbor	loop	MI	ACC	SEN	SPE	AUC
sMCI vs. pMCI	✓			0.810	0.696	0.857	0.831
	✓			0.835	0.674	0.902	0.842
			✓	0.845	0.662	0.920	0.849
		✓	✓	0.836	0.640	0.916	0.846
		✓	✓	0.850	0.636	0.938	0.855
	✓	✓	✓	0.839	0.644	0.918	0.851
	✓	✓	✓	0.858	0.717	0.936	0.860
sNC vs. pNC	✓			0.880	0.861	0.893	0.922
	✓			0.889	0.847	0.918	0.934
			✓	0.904	0.889	0.914	0.936
		✓	✓	0.882	0.824	0.922	0.929
		✓	✓	0.894	0.868	0.911	0.895
	✓	✓	✓	0.896	0.878	0.908	0.921
	✓	✓	✓	0.917	0.874	0.947	0.949

MSA3D [10] implemented a slice-level attention and a 3D CNN to capture subject-level structural changes; 7) M²FAN [11] designed modules of weakly supervised meta-information learning to learn and disentangle meta-information from class-related representations; 8) DH-ProGCN [26] constructed hierarchical structure brain networks for classification.

The comparisons between Brain-SubGNN and existing SOTA methods are presented in Tab.II. Notably, Brain-SubGNN demonstrates superior performance in MCI conversion prediction, achieving ACC=0.869 and AUC=0.882 in tests conducted on the ADNI-2, with models trained on ADNI-1.

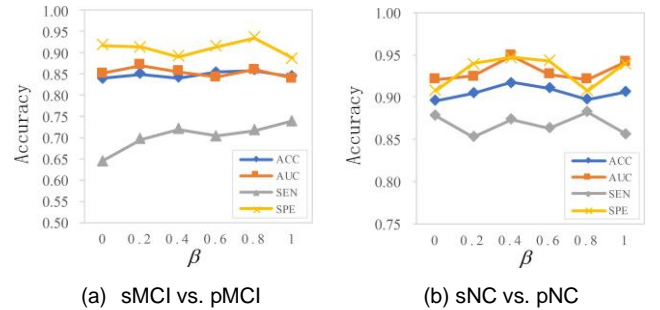


Fig. 5. Effects of the coefficient of MI module in controlling the contribution of the Global-Aware MI loss.

D. Effectiveness of Dynamic Brain Network Construction

1) *Dynamic critical region exploring*: To validate the effectiveness of dynamic critical region exploration, we compared 1) the ROI-based approach, choose 90 regions of AAL as nodes; 2) the backbone network without channel clustering; and 3) the backbone network with channel clustering (i.e., dynamic node). As shown in Tab.III, the dynamic clustering outperforms the ROI and backbone based approaches in terms of MCI conversion and can produce better feature distributions for downstream brain image analysis tasks.

2) *Dynamic edge connection*: To verify whether our constructed dynamic brain network outperforms the fixed structure, we directly connect all critical region nodes after channel clustering and input them into a two-layer GNN for classification to obtain a fixed brain network map. The results are shown in Tab.III, where the dynamic brain network structure performs better, indicating that dynamic measurement of inter-regional correlations is necessary to construct the brain network.

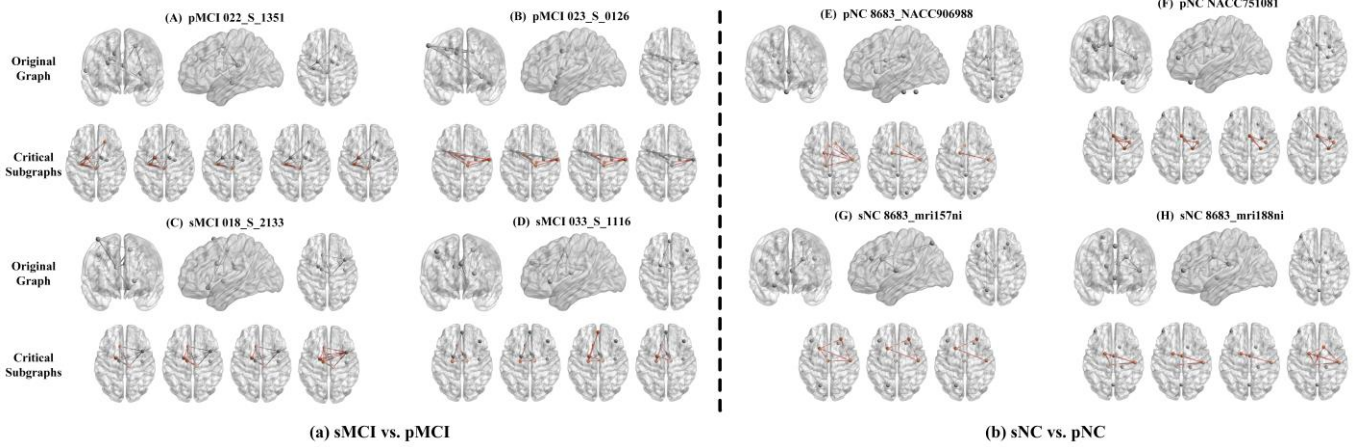


Fig. 6. Visualization of the constructed original graphs and the mined critical subgraphs. (A)-(D) and (E)-(H) are the visualizations of MCI and NC subjects, respectively.

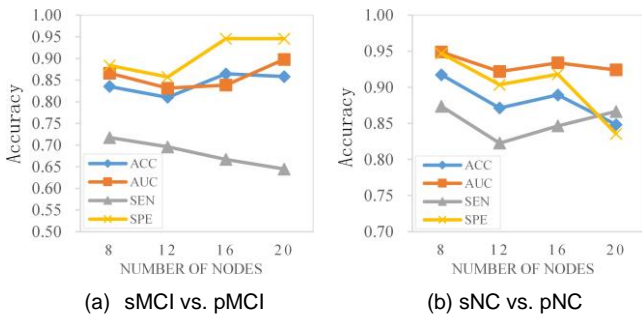


Fig. 7. Effects of the number of nodes in constructing the brain network graph on the results with 5-fold cross-validated

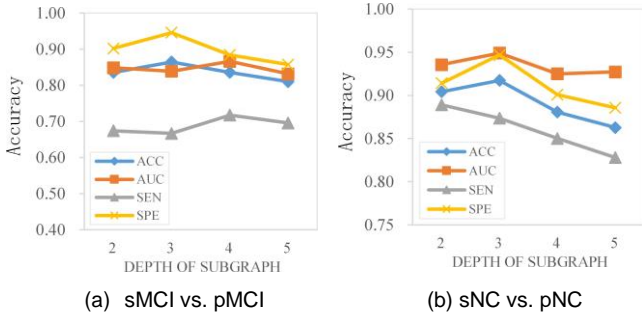


Fig. 8. Effects of the depth of subgraph in mining the brain network representation with 5-fold cross-validated.

E. Effectiveness of Critical Subgraph Mining

1) **Subgraph mining:** The results of the ablation experiments for subgraph mining on two tasks are summarized in rows 2, 4 and 6 of Tab.IV. The experiments reveal a sequential increase in average accuracy from the baseline to the incorporation of loop and neighbor subgraph mining modules, both individually and in combination. This consistent improvement supports the effectiveness of our critical subgraph mining strategy, emphasizing the Subgraph Reinforced Mining Module's role in improving graph classification by extracting more meaningful and predictive subgraphs.

2) **Subgraph representation enhancement:** Rows 3, 5 and 7 of Tab.IV summarizes the results of the ablation studies focusing on the subgraph representation enhancement module for two tasks. These results with MI enhancement in subgraph mining modules are better than those without it. for two tasks.

3) **MI Coefficient:** The sensitivity of the MI loss coefficient β is designed for controlling the contribution of the Global-Aware MI loss L_{global} , and analyzed across two datasets in (16). As observed in Fig.5, Brain-SubGNN achieves optimal on both datasets when β ranges 0.4 to 0.6. This indicates that embedding overall graph properties into subgraphs is particularly beneficial for brain network analysis. The proposed MI enhancement mechanism is adept at capturing diverse critical information specific to different dataset types.

F. Effectiveness of Graph and Subgraph Representation

1) **Size of Brain Graph:** To find the optimal graph representation of the brain network, we investigated how the size of the graph affects the performance of Brain-SubGNN. As described in Section III-A, the number of nodes can be adjusted by controlling the number of channel clustering centers. The experimental results show that both too large and too small graph sizes degrade the performance of Brain-SubGNN. As shown in Fig.7, the best graph size of sMCI vs. pMCI and sNC vs. pNC (average number of vertices $N=16$) has the best performance compared with others. Too few nodes may over-generalize by encompassing excessive regions, thus limiting local specificity; whereas too many nodes might overly emphasize local variations, reducing the overall accuracy of the evaluation.

2) **Maximum Depth of Subgraph:** In Fig.8, we evaluate the proposed Brain-SubGNN with different maximum subgraph depths K from 2 to 5 on sMCI vs. pMCI and sNC vs. pNC tasks. K determines the agent state as well as the range of the action set. As shown in Fig.8a and 8b, Brain-SubGNN achieves the best performance with $K=3$ in sMCI vs. pMCI and sNC vs. pNC. This indicates that the critical subgraphs in MCI subject networks have a higher order than in NC subject networks.

This is logical, as pNC lesions are typically micro-localized, while MCI involves broader brain connectivity, affecting deterioration prediction. Hence, Brain-SubGNN excels when critical subgraphs encapsulate vital functional elements of the graph, balancing local and global analysis.

G. Visualization

We present a visualization of the brain networks and their

corresponding critical subgraphs for both the sMCI vs. pMCI and sNC vs. pNC tasks in Fig.6. The original graphs are the brain networks constructed by Section.III-A, while the critical subgraphs are mined by the subgraph mining module.

Our framework identifies several critical regions and structures within the brain networks that are consistent with current neurological research. For instance, in the case of sMCI vs. pMCI tasks, the critical subgraphs prominently feature regions such as the hippocampus and the entorhinal cortex [70]-[71], which are known to be affected in the early stages of MCI and AD. Furthermore, our framework highlights a notable pattern of connectivity between the frontal lobe and the temporal lobe in the sNC vs. pNC tasks. The visualization reveals a decrease in connectivity in these regions in subjects progressing from sNC to pNC. This observation echoes recent theories [72] suggesting the importance of frontal-temporal connections in the maintenance of cognitive functions, particularly in the context of normal aging.

These results not only demonstrate the efficacy of our Brain-SubGNN framework in accurately identifying critical regions and structures but also validate its potential as a tool for neuroscientific research. By aligning our findings with existing neurological theories, we establish a credible foundation for the interpretation of our results, offering a promising avenue for further exploration in the domain of brain network analysis.

V. CONCLUSION

This work presents a framework for constructing dynamic structure brain networks from T1-MRI, emphasizing critical subgraph mining and enhancement with a novel graph representation framework Brain-SubGNN. The method begins with feature extraction using a convolutional network, followed by constructing the brain network using a correlation matrix between nodes. Then, Brain-SubGNN adaptively mines and enhances data-specific critical subgraphs, capturing both loop and neighbor subgraphs to reflect long-range and local connections, while maintaining the network's local and global attributes. Offering explicit subgraph-level interpretation rather than node- or edge-level interpretation, Brain-SubGNN provides enhanced insights into graph analysis, marking a significant advancement in neuroimaging and cognitive disorder research.

REFERENCES

- [1] A. Metastasio, P. Rinaldi, R. Tarducci, E. Mariani, F. T. Feliziani, A. Cherubini, G. P. Pelliccioli, G. Gobbi, U. Senin, and P. Mecocci, "Conversion of mci to dementia: role of proton magnetic resonance spectroscopy," *Neurobiology of aging*, vol. 27, no. 7, pp. 926–932, 2006.
- [2] L. Yue, Y. Pan, T. Wang, M. Liu, D. Shen, and S. Xiao, "Characterizing mri biomarkers for early prediction of amnesic mild cognitive impairment among the community-dwelling chinese: Neuroimaging/optimal neuroimaging measures for early detection," *Alzheimer's & Dementia*, vol. 16, p. e041450, 2020.
- [3] G. B. Frisoni, N. C. Fox, C. R. Jack Jr, P. Scheltens, and P. M. Thompson, "The clinical use of structural mri in alzheimer disease," *Nature Reviews Neurology*, vol. 6, no. 2, pp. 67–77, 2010.
- [4] A. Chincarini, P. Bosco, P. Calvini, G. Gemme, M. Esposito, C. Olivieri, L. Rei, S. Squarcia, G. Rodriguez, R. Bellotti et al., "Local mri analysis approach in the diagnosis of early and prodromal alzheimer's disease," *Neuroimage*, vol. 58, no. 2, pp. 469–480, 2011.
- [5] M. Liu, J. Zhang, E. Adeli, and D. Shen, "Landmark-based deep multi-instance learning for brain disease diagnosis," *Medical image analysis*, vol. 43, pp. 157–168, 2018.
- [6] C. Lian, M. Liu, Y. Pan, and D. Shen, "Attention-guided hybrid network for dementia diagnosis with structural mr images," *IEEE transactions on cybernetics*, vol. 52, no. 4, pp. 1992–2003, 2020.
- [7] Y. Pan, M. Liu, Y. Xia, and D. Shen, "Disease-image-specific learning for diagnosis-oriented neuroimage synthesis with incomplete multi-modality data," *IEEE transactions on pattern analysis and machine intelligence*, vol. 44, no. 10, pp. 6839–6853, 2021.
- [8] C. Lian, M. Liu, J. Zhang, and D. Shen, "Hierarchical fully convolutional network for joint atrophy localization and alzheimer's disease diagnosis using structural mri," *IEEE transactions on pattern analysis and machine intelligence*, vol. 42, no. 4, pp. 880–893, 2018.
- [9] H. Guan, Y. Liu, E. Yang, P.-T. Yap, D. Shen, and M. Liu, "Multi-site mri harmonization via attention-guided deep domain adaptation for brain disorder identification," *Medical image analysis*, vol. 71, p. 102076, 2021.
- [10] L. Chen, H. Qiao, and F. Zhu, "Alzheimer's disease diagnosis with brain structural mri using multiview-slice attention and 3d convolution neural network," *Frontiers in Aging Neuroscience*, vol. 14, 2022.
- [11] K. Han, G. Li, Z. Fang, and F. Yang, "Multi-template meta-information regularized network for alzheimer's disease diagnosis using structural mri," *IEEE Transactions on Medical Imaging*, 2023.
- [12] J. Zhang, X. He, L. Qing, X. Chen, Y. Liu, and H. Chen, "Multi-relation graph convolutional network for alzheimer's disease diagnosis using structural mri," *Knowledge-Based Systems*, vol. 270, p. 110546, 2023.
- [13] Y. Zhu, J. Ma, C. Yuan, and X. Zhu, "Interpretable learning based dynamic graph convolutional networks for alzheimer's disease analysis," *Information Fusion*, vol. 77, pp. 53–61, 2022.
- [14] E. Bullmore and O. Sporns, "Complex brain networks: graph theoretical analysis of structural and functional systems," *Nature reviews neuroscience*, vol. 10, no. 3, pp. 186–198, 2009.
- [15] M. Thiebaut de Schotten and S. J. Forkel, "The emergent properties of the connected brain," *Science*, vol. 378, no. 6619, pp. 505–510, 2022.
- [16] M. Axer and K. Amunts, "Scale matters: The nested human connectome," *Science*, vol. 378, no. 6619, pp. 500–504, 2022.
- [17] U. Alvarez-Rodriguez, F. Battiston, G. F. de Arruda, Y. Moreno, M. Perc, and V. Latora, "Evolutionary dynamics of higher-order interactions in social networks," *Nature Human Behaviour*, vol. 5, no. 5, pp. 586–595, 2021.
- [18] J. Chen, L. Zheng, Y. Hu, W. Wang, H. Zhang, and X. Hu, "Traffic flow matrix-based graph neural network with attention mechanism for traffic flow prediction," *Information Fusion*, vol. 104, p. 102146, 2024.
- [19] X. Fang, L. Liu, J. Lei, D. He, S. Zhang, J. Zhou, F. Wang, H. Wu, and H. Wang, "Geometry-enhanced molecular representation learning for property prediction," *Nature Machine Intelligence*, vol. 4, no. 2, pp. 127–134, 2022.
- [20] X. Song, F. Zhou, A. F. Frangi, J. Cao, X. Xiao, Y. Lei, T. Wang, and B. Lei, "Graph convolution network with similarity awareness and adaptive calibration for disease-induced deterioration prediction," *Medical Image Analysis*, vol. 69, p. 101947, 2021.
- [21] Y. Chen, J. Yan, M. Jiang, T. Zhang, Z. Zhao, W. Zhao, J. Zheng, D. Yao, R. Zhang, K. M. Kendrick et al., "Adversarial learning based node-edge graph attention networks for autism spectrum disorder identification," *IEEE Transactions on Neural Networks and Learning Systems*, 2022.
- [22] X. Song, F. Zhou, A. F. Frangi, J. Cao, X. Xiao, Y. Lei, T. Wang, and B. Lei, "Multi-center and multi-channel pooling gcnn for early ad diagnosis based on dual-modality fused brain network," *IEEE Transactions on Medical Imaging*, 2022.
- [23] B. Lei, N. Cheng, A. F. Frangi, E.-L. Tan, J. Cao, P. Yang, A. Elazab, J. Du, Y. Xu, and T. Wang, "Self-calibrated brain network estimation and joint non-convex multi-task learning for identification of early alzheimer's disease," *Medical image analysis*, vol. 61, p. 101652, 2020.
- [24] Y. Li, Q. Wei, E. Adeli, K. M. Pohl, and Q. Zhao, "Joint graph convolution for analyzing brain structural and functional connectome," in *Medical Image Computing and Computer Assisted Intervention– MICCAI 2022: 25th International Conference, Singapore, September 18–22, 2022, Proceedings, Part I*. Springer, 2022, pp. 231–240.
- [25] F. S. Duran, A. Beyaz, and I. Rekić, "Dual-hinet: Dual hierarchical integration network of multigraphs for connectional brain template learning," in *Medical Image Computing and Computer Assisted Intervention–*

- MICCAI 2022: 25th International Conference, Singapore, September 18–22, 2022, Proceedings, Part I. Springer, 2022, pp. 305–314.
- [26] Y. Leng, W. Cui, C. Bai, Z. Chen, Y. Zheng, and J. Zheng, “Dynamic structural brain network construction by hierarchical prototype embedding gcn using t1-mri,” in International Conference on Medical Image Computing and Computer-Assisted Intervention. Springer, 2023, pp. 120–130.
- [27] H. Cui, W. Dai, Y. Zhu, X. Li, L. He, and C. Yang, “Brainnexplainer: An interpretable graph neural network framework for brain network based disease analysis,” arXiv preprint arXiv:2107.05097, 2021.
- [28] X. Kan, H. Cui, J. Lukemire, Y. Guo, and C. Yang, “Fbnetgen: Task-aware gnn-based fmri analysis via functional brain network generation,” in International Conference on Medical Imaging with Deep Learning. PMLR, 2022, pp. 618–637.
- [29] Y. Zhu, H. Cui, L. He, L. Sun, and C. Yang, “Joint embedding of structural and functional brain networks with graph neural networks for mental illness diagnosis,” in 2022 44th Annual International Conference of the IEEE Engineering in Medicine & Biology Society (EMBC). IEEE, 2022, pp. 272–276.
- [30] H. Cui, W. Dai, Y. Zhu, X. Li, L. He, and C. Yang, “Interpretable graph neural networks for connectome-based brain disorder analysis,” in International Conference on Medical Image Computing and Computer-Assisted Intervention. Springer, 2022, pp. 375–385.
- [31] N. M. Kriege, F. D. Johansson, and C. Morris, “A survey on graph kernels,” *Applied Network Science*, vol. 5, no. 1, pp. 1–42, 2020.
- [32] N. Shervashidze, P. Schweitzer, E. J. Van Leeuwen, K. Mehlhorn, and K. M. Borgwardt, “Weisfeiler-lehman graph kernels.” *Journal of Machine Learning Research*, vol. 12, no. 9, 2011.
- [33] D. Chen, L. O’Bray, and K. Borgwardt, “Structure-aware transformer for graph representation learning,” in International Conference on Machine Learning. PMLR, 2022, pp. 3469–3489.
- [34] S. Geisler, Y. Li, D. J. Mankowitz, A. T. Cemgil, S. Gu’nnemann, and C. Paduraru, “Transformers meet directed graphs,” in International Conference on Machine Learning. PMLR, 2023, pp. 11 144–11 172.
- [35] R. Sitaram, T. Ros, L. Stoeckel, S. Haller, F. Scharnowski, J. Lewis-Peacock, N. Weiskopf, M. L. Belfari, M. Rana, E. Oblak et al., “Closed-loop brain training: the science of neurofeedback,” *Nature Reviews Neuroscience*, vol. 18, no. 2, pp. 86–100, 2017.
- [36] S. Skouras, J. Torner, P. Andersson, Y. Koush, C. Falcon, C. Minguillon, K. Fauria, F. Alpile, K. Blenow, H. Zetterberg et al., “Earliest amyloid and tau deposition modulate the influence of limbic networks during closed-loop hippocampal downregulation,” *Brain*, vol. 143, no. 3, pp. 976–992, 2020.
- [37] M. P. Van Den Heuvel and O. Sporns, “Rich-club organization of the human connectome,” *Journal of Neuroscience*, vol. 31, no. 44, pp. 15 775–15 786, 2011.
- [38] D. S. Bassett and E. Bullmore, “Small-world brain networks,” *The neuroscientist*, vol. 12, no. 6, pp. 512–523, 2006.
- [39] J. Ashburner and K. J. Friston, “Voxel-based morphometry—the methods,” *Neuroimage*, vol. 11, no. 6, pp. 805–821, 2000.
- [40] D. Zhang, Y. Wang, L. Zhou, H. Yuan, D. Shen, A. D. N. Initiative et al., “Multimodal classification of alzheimer’s disease and mild cognitive impairment,” *Neuroimage*, vol. 55, no. 3, pp. 856–867, 2011.
- [41] M. M. Bronstein, J. Bruna, Y. LeCun, A. Szlam, and P. Vandergheynst, “Geometric deep learning: going beyond euclidean data,” *IEEE Signal Processing Magazine*, vol. 34, no. 4, pp. 18–42, 2017.
- [42] T. Gartner, P. Flach, and S. Wrobel, “On graph kernels: Hardness results and efficient alternatives,” in Learning Theory and Kernel Machines: 16th Annual Conference on Learning Theory and 7th Kernel Workshop, COLT/Kernel 2003, Washington, DC, USA, August 24–27, 2003. Proceedings. Springer, 2003, pp. 129–143.
- [43] Y. Wang, Y.-Y. Chang, Y. Liu, J. Leskovec, and P. Li, “Inductive representation learning in temporal networks via causal anonymous walks,” International Conference on Learning Representations, 2021.
- [44] K. M. Borgwardt and H.-P. Kriegel, “Shortest-path kernels on graphs,” in Fifth IEEE international conference on data mining (ICDM’05). IEEE, 2005, pp. 8–pp.
- [45] Y. Luo and P. Li, “Neighborhood-aware scalable temporal network representation learning,” in Learning on Graphs Conference. PMLR, 2022, pp. 1–1.
- [46] W. Cong, S. Zhang, J. Kang, B. Yuan, H. Wu, X. Zhou, H. Tong, and M. Mahdavi, “Do we really need complicated model architectures for temporal networks?” arXiv preprint arXiv:2302.11636, 2023.
- [47] Z. Tang, T. Li, D. Wu, J. Liu, and Z. Yang, “A systematic literature review of reinforcement learning-based knowledge graph research,” *Expert Systems with Applications*, p. 121880, 2023.
- [48] K.-H. Lai, D. Zha, K. Zhou, and X. Hu, “Policy-gnn: Aggregation optimization for graph neural networks,” in Proceedings of the 26th ACM SIGKDD International Conference on Knowledge Discovery & Data Mining, 2020, pp. 461–471.
- [49] H. Xu, Y. Ma, H.-C. Liu, D. Deb, H. Liu, J.-L. Tang, and A. K. Jain, “Adversarial attacks and defenses in images, graphs and text: A review,” *International Journal of Automation and Computing*, vol. 17, pp. 151–178, 2020.
- [50] S. Zhu, I. Ng, and Z. Chen, “Causal discovery with reinforcement learning,” arXiv preprint arXiv:1906.04477, 2019.
- [51] H. Yuan, H. Yu, J. Wang, K. Li, and S. Ji, “On explainability of graph neural networks via subgraph explorations,” in International conference on machine learning. PMLR, 2021, pp. 12 241–12 252.
- [52] N. Mazyavkina, S. Sviridov, S. Ivanov, and E. Burnaev, “Reinforcement learning for combinatorial optimization: A survey,” *Computers & Operations Research*, vol. 134, p. 105400, 2021.
- [53] Z. Wang and S. Ji, “Second-order pooling for graph neural networks,” *IEEE Transactions on Pattern Analysis and Machine Intelligence*, 2020.
- [54] Y. Dou, Z. Liu, L. Sun, Y. Deng, H. Peng, and P. S. Yu, “Enhancing graph neural network-based fraud detectors against camouflaged fraudsters,” in Proceedings of the 29th ACM international conference on information & knowledge management, 2020, pp. 315–324.
- [55] H. Peng, R. Zhang, S. Li, Y. Cao, S. Pan, and S. Y. Philip, “Reinforced, incremental and cross-lingual event detection from social messages,” *IEEE Transactions on Pattern Analysis and Machine Intelligence*, vol. 45, no. 1, pp. 980–998, 2022.
- [56] V. Mnih, K. Kavukcuoglu, D. Silver, A. A. Rusu, J. Veness, M. G. Bellemare, A. Graves, M. Riedmiller, A. K. Fidjeland, G. Ostrovski et al., “Human-level control through deep reinforcement learning,” *nature*, vol. 518, no. 7540, pp. 529–533, 2015.
- [57] Y. Gao, H. Yang, P. Zhang, C. Zhou, and Y. Hu, “Graphnas: Graph neural architecture search with reinforcement learning,” arXiv preprint arXiv:1904.09981, 2019.
- [58] H. Zheng, J. Fu, T. Mei, and J. Luo, “Learning multi-attention convolutional neural network for fine-grained image recognition,” in Proceedings of the IEEE international conference on computer vision, 2017, pp. 5209–5217.
- [59] S. Lloyd, “Least squares quantization in pcm,” *IEEE transactions on information theory*, vol. 28, no. 2, pp. 129–137, 1982.
- [60] J. Li, P. Zhou, C. Xiong, and S. C. Hoi, “Prototypical contrastive learning of unsupervised representations,” arXiv preprint arXiv:2005.04966, 2020.
- [61] A. Vaswani, N. Shazeer, N. Parmar, J. Uszkoreit, L. Jones, A. N. Gomez, L. Kaiser, and I. Polosukhin, “Attention is all you need,” *Advances in neural information processing systems*, vol. 30, 2017.
- [62] S. Nowozin, B. Cseke, and R. Tomioka, “f-gan: Training generative neural samplers using variational divergence minimization,” *Advances in neural information processing systems*, vol. 29, 2016.
- [63] R. D. Hjelm, A. Fedorov, S. Lavoie-Marchildon, K. Grewal, P. Bachman, A. Trischler, and Y. Bengio, “Learning deep representations by mutual information estimation and maximization,” arXiv preprint arXiv:1808.06670, 2018.
- [64] R. C. Petersen, P. S. Aisen, L. A. Beckett, M. C. Donohue, A. C. Gamst, D. J. Harvey, C. R. Jack, W. J. Jagust, L. M. Shaw, A. W. Toga et al., “Alzheimer’s disease neuroimaging initiative (adni): clinical characterization,” *Neurology*, vol. 74, no. 3, pp. 201–209, 2010.
- [65] L. Besser, W. Kukull, D. S. Knopman, H. Chui, D. Galasko, S. Weintraub, G. Jicha, C. Carlsson, J. Burns, J. Quinn et al., “Version 3 of the national alzheimer’s coordinating center’s uniform data set,” *Alzheimer Disease & Associated Disorders*, vol. 32, no. 4, pp. 351–358, 2018.
- [66] A. Trockman and J. Z. Kolter, “Patches are all you need?” arXiv preprint arXiv:2201.09792, 2022.
- [67] X. Chen, H. Fan, R. Girshick, and K. He, “Improved baselines with momentum contrastive learning,” arXiv preprint arXiv:2003.04297, 2020.
- [68] G. Li, M. Müller, G. Qian, I. C. D. Perez, A. Abualshour, A. K. Thabet, and B. Ghanem, “Deepgcns: Making gcns go as deep as cnns,” *IEEE transactions on pattern analysis and machine intelligence*, 2021.
- [69] K. Xu, W. Hu, J. Leskovec, and S. Jegelka, “How powerful are graph neural networks?” arXiv preprint arXiv:1810.00826, 2018.
- [70] A. Du, N. Schuff, D. Amend, M. Laakso, Y. Hsu, W. Jagust, K. Yaffe, J. Kramer, B. Reed, D. Norman et al., “Magnetic resonance imaging of the entorhinal cortex and hippocampus in mild cognitive impairment and

- alzheimer's disease," *Journal of Neurology, Neurosurgery & Psychiatry*, vol. 71, no. 4, pp. 441–447, 2001.
- [71] L. Pini, M. Pievani, M. Bocchetta, D. Altomare, P. Bosco, E. Cavedo, S. Galluzzi, M. Marizzoni, and G. B. Frisoni, "Brain atrophy in alzheimer's disease and aging," *Ageing research reviews*, vol. 30, pp. 25–48, 2016.
- [72] B. M. Hampstead, A. Y. Stringer, A. D. Jordan, R. Ploutz-Snyder, and K. Sathian, "Toward rational use of cognitive training in those with mild cognitive impairment," *Alzheimer's & Dementia*, vol. 19, no. 3, pp. 933–945, 2023.